



CHORUS

This is the accepted manuscript made available via CHORUS. The article has been published as:

Structural, vibrational, and thermodynamic properties of ordered and disordered $\text{Ni}_{1-x}\text{Pt}_x$ alloys from first-principles calculations

S. L. Shang, Y. Wang, D. E. Kim, C. L. Zacherl, Y. Du, and Z. K. Liu

Phys. Rev. B **83**, 144204 — Published 18 April 2011

DOI: [10.1103/PhysRevB.83.144204](https://doi.org/10.1103/PhysRevB.83.144204)

Structural, vibrational, and thermodynamic properties of ordered and disordered $\text{Ni}_{1-x}\text{Pt}_x$ alloys from first-principles calculations

S. L. Shang,^{1,*} Y. Wang,¹ D. E. Kim,¹ C. L. Zacherl,¹ Y. Du,² and Z. K. Liu¹

¹*Department of Materials Science and Engineering, The Pennsylvania State University,
University Park, Pennsylvania 16802, USA*

²*State Key Laboratory of Powder Metallurgy, Central South University, Changsha, Hunan
410083, China*

In terms of first-principles phonon calculations and quasiharmonic approach, the structural, vibrational, and thermodynamic properties have been investigated for the ordered and disordered $\text{Ni}_{1-x}\text{Pt}_x$ alloys with the main focus being on the disordered $\text{Ni}_{0.5}\text{Pt}_{0.5}$. To gain insight into the disordered alloys, we use special quasirandom structures (SQS's) and demonstrate their capabilities in predicting (i) the bond length distributions, (ii) the phonon spectra, and (iii) the elastic stiffness constants of the disordered alloys. It is found that the Pt-Pt atomic pairs possess the longest bond lengths relative to the Ni-Pt and Ni-Ni ones in the disordered alloys, the predicted force constants indicate that the Pt-Pt bond is stiffer when compared to the Ni-Pt and the Ni-Ni ones for both the ordered and disordered alloys, and the phonon density of states of the disordered alloys are similar to the broadened versions of the ordered cases. Based on the results of the ordered and disordered alloys, a slightly positive deviation from Vegard's law is found for the volume variation of $\text{Ni}_{1-x}\text{Pt}_x$, and correspondingly, a negative deviation is predicted for the change of bulk modulus. With increasing Pt content, the bulk modulus derivative relative to pressure increases approximately linearly, whereas the magnetic moment decreases. In addition,

the SQS predicted relative energies (enthalpies of formation) for the disordered $\text{Ni}_{1-x}\text{Pt}_x$ are also compared to cluster expansion predictions. As an application of the finite temperature thermodynamic properties, the phase transition between the ordered L1_0 and the disordered $\text{Ni}_{0.5}\text{Pt}_{0.5}$ is predicted to be 755 ± 128 K, which agrees reasonably well with the measurement around 900 K, demonstrating that the driving force of the phase transition stems mainly from the configurational entropy rather than the vibrational entropy.

PACS numbers: 63.50.Gh, 65.40.G-, 62.20.D-, 71.20.Be

I. INTRODUCTION

Thermal barrier coating (TBC) systems are widely used to increase further the operating temperatures of gas turbine engines (increasing ~ 150 K, thereby improves the efficiency of energy conversion) and to protect metal components such as turbine blades and vanes from the hot combustion gases.¹⁻² It is believed that the life time of the TBC systems is ultimately limited by the failure of the bond coat within, i.e., the development of cracks caused by oxidation of the bond coat.³⁻⁴ The Ni-Pt system is crucial in the development of bond coat alloys, such as the Pt modified β -NiAl,¹ and the one recently developed based on the two-phase mixture of γ -Ni + γ' -Ni₃Al in the Ni-Al-Pt based system by Gleeson et al.⁵⁻⁶ Besides the technologically important Ni-Pt system for bond coat, Ni_{1-x}Pt_x is a well studied disordered alloy both experimentally and theoretically due to its simple fcc structure over a wide composition range,⁷ and can be grown easily at nearly any concentration. In order to design novel bond coat for the TBC systems and in particular to probe the theoretical methodology for the disordered alloys, the present work investigates the structural, phonon, and thermodynamic properties of the ordered and disordered Ni_{1-x}Pt_x alloys through first-principles calculations.

Despite years of research efforts, structural/theoretical model of the substitutionally disordered (random) alloy still remains one of the least explored issues in first-principles community due to the uncertainty about atomic occupations, such as the positions of A and B atoms in a disordered A_{1-x}B_x alloy. Currently three approaches stand out among first-principles models for disordered alloys.⁸ Each has its own advantages and disadvantages. The first approach is the coherent potential approximation (CPA),⁹ where the average occupations of A and B atoms are assumed in a structureless uniform average medium.¹⁰ Therefore, local structural relaxations are excluded

in CPA, which contrasts with the experimental observations because distances between A-A, B-B, and A-B atoms are generally different.¹¹⁻¹² The second approach is the cluster expansion method (CEM),¹³⁻¹⁵ which is driven from statistical lattice theory about the one-to-one correspondence between a given structure and a set of correlation functions. The configuration-dependent properties of ordered and disordered alloys are determined from the correlation functions of the phase of interest and the effective cluster interactions (ECI's). It is worth mentioning that the ECI's are estimated from a variety of ordered structures, but are useable for both ordered and disordered structures. Note that the truncated error in determining ECI's is unavoidable (see the present Ni-Pt case below), and the local structural information of the disordered structure is also excluded in CEM. The third approach is the special quasirandom structure (SQS) proposed by Zunger et al.,¹⁰ which is driven from the same origin as in the CEM approach, i.e., a given structure can be characterized by a set of correlation functions. Essentially, SQS is an ordered supercell with a few (e.g., 4~32) atoms that mimic the most relevant pair and multisite correlation functions of the disordered phase. In contrast to the global and nonstructural natures of CPA and CEM, SQS is a local structural model, giving one of the down-selected microstates of disordered phase. Regarding the first-principles research on the disordered Ni_{1-x}Pt_x alloys, attempts have been made using CPA and the itinerant CPA methods to study the phonon properties.¹⁶⁻¹⁷ However, the CPA-type methods are excluded herein because they are incapable of capturing the intrinsic nature of disordered alloys. Instead, CEM and SQS method will be used in the present work with most of the focus on the SQS calculations. Previously, the SQS method was used extensively to study the electronic structures and thermodynamic properties of the disordered alloys (see such as Refs. 8, 10, 18-21). Using the SQS method, studies have also been performed to calculate the phonon properties of disordered alloys, e.g., Pd₃V,²² Ni₃Al,²³ In_xGa_{1-x}.

$x\text{N}$,²⁴ and $\text{Ga}_{0.5}\text{In}_{0.5}\text{P}$.²⁵ However, ≤ 8 random atoms were included in these SQS phonon calculations, and a detailed analysis of phonon properties was absent. In an effort to gain insight into the properties of the disordered $\text{Ni}_{1-x}\text{Pt}_x$ and to demonstrate the capabilities of the SQS method, the present work primarily uses the first-principles SQS method to predict (i) the bond length distributions, (ii) the phonon properties, and (iii) the elastic constants of the disordered $\text{Ni}_{1-x}\text{Pt}_x$. Together with the results from the ordered alloys (compounds), the regularities of the structural, vibrational, and thermodynamic properties of the $\text{Ni}_{1-x}\text{Pt}_x$ alloys are investigated and compared with experimental data when possible.

The remainder of this paper is organized as follows. In Sec. II, we present the ordered compounds and disordered SQS structures used for the fcc based $\text{Ni}_{1-x}\text{Pt}_x$ alloys and the details of the first-principles and phonon calculations. In Sec. III, we discuss the predicted properties of $\text{Ni}_{1-x}\text{Pt}_x$ alloys, including (i) the bond length distributions of the disordered $\text{Ni}_{1-x}\text{Pt}_x$, (ii) the elastic constants of the disordered $\text{Ni}_{0.5}\text{Pt}_{0.5}$, (iii) the equilibrium structural properties including volume, bulk modulus, the pressure derivative of the bulk modulus, magnetic moment, and relative energy for ordered and disordered $\text{Ni}_{1-x}\text{Pt}_x$, (iv) the phonon density of states and force constants of the ordered and disordered $\text{Ni}_{0.5}\text{Pt}_{0.5}$, and (v) the phase transition between the ordered L1_0 and the disordered $\text{Ni}_{0.5}\text{Pt}_{0.5}$ structures. Finally, in Sec. IV the conclusions of the present work are given.

II. THEORY AND METHODOLOGY

A. Disordered and ordered structures

As mentioned in Sec. I, there exists a one-to-one correspondence between a given structure and a set of correlation functions, which is the key for both the CEM and SQS methods.^{10, 13-15} In the case of a binary alloy, the correlation function $\Pi_{k,l}$ for a figure (cluster) $f(k,l)$ with k vertices and separated by an l^{th} neighbor distance is defined as follows,¹³

$$\text{Eq. 1} \quad \Pi_{k,l} = \frac{1}{N_{k,l}} \sum_{\{k,l\}} \sigma_1 \sigma_2 \cdots \sigma_k$$

where σ_k is a spin-like variable which takes the value of +1 or -1 depending on whether the atomic site is occupied by an A or B atom. The sum is over all of the $f(k,l)$ clusters with $N_{k,l}$ being the total number of such clusters. For a disordered alloy of $A_{1-x}B_x$, Eq. 1 reduces to $\Pi_{k,l} = (2x - 1)^k$. In order to generate the SQS for a given number of atoms, we need to find an ordered structure from all the possible structure configurations, where the obtained ordered structure (i.e., SQS) has the most relevant pair and multisite correlation functions of the disordered phase.¹⁰ Therefore, the essence of SQS is to use an *ordered* structure to mimic the properties of the corresponding *disordered* structure. For fcc based binary systems, the SQS's have been reported for the 8-atom (SQS-8),²⁰⁻²¹ 16-atom (SQS-16),²⁶ 32-atom (SQS-32),^{8, 27} and even 48-atom (SQS-48)²⁷ cases. We argue that the reported SQS-32 structures are in fact near-SQS's rather than SQS's, since the authors^{8, 27} did not search all of the possible configurations (note that we did not check the reported SQS-48's). For the near SQS-32's with compositions $x = 0.25$ and 0.5 reported by Ghosh et al.,⁸ the pair correction functions are equal those of the disordered cases from the first to the forth-nearest neighbor only. For the near SQS-32 ($x = 0.25$) reported by Ruban et al.,²⁷ only the first and second pair correction functions are equal to those of the disordered cases. Using the ATAT code (improved by present author YW),²⁸ we search all the possible configurations and generate the fcc based 8-, 16-, and 32-atom SQS's with the

compositions $x = 0.25$ and 0.5 (see Appendix for the structure details). In Table 1, the pair correlation functions $\Pi_{2,l}$ (l up to the 11th nearest neighbor) of these fcc based SQS's generated in the present work are reported. For SQS-32 with $x = 0.25$, the $\Pi_{2,l}$'s mimic the disordered ones for $l = 1\sim 7$; and $l = 1\sim 8$ for SQS-32 with $x = 0.5$. Clearly, based on the criterion of pair correlation functions, the SQS-32 structures generated in the present work are closer to the disordered case than the ones previously reported in the literature.^{8,27}

For the fcc based ordered structures, we employ all of the A_mB_n structures with $m, n = 0, 1, \dots, 4$, and $m + n \leq 4$, with the total number of structures being 29. Note that these structures are generated by the ATAT code.²⁸ In addition, we also choose 8 A_mB_n structures with $5 \leq m+n \leq 8$, i.e., the mC10, D1_a, D1/D7, and the ACS structure.²⁹ The structure details and the commonly used names²⁹⁻³¹ for these 37 structures are given in the Appendix.

B. First-principles and phonon calculations

In the present work the first-principles calculations are performed using the VASP code,³²⁻³³ with the ion-electron interaction described by the projector augmented wave (PAW) method.³⁴ The selection of the PAW method rather than the ultrasoft pseudo-potential is due to the fact that the PAW method combines the accuracy of all-electron methods with the efficiency of pseudo-potential.³⁴⁻³⁵ Regarding the exchange-correction functional, the generalized gradient approximation (GGA)³⁶ is used instead of the local density approximation (LDA),³⁷⁻³⁸ since GGA describes Ni and Ni-based alloys well (see Sec. III for more details). In the VASP calculations, the samplings of k-points are at least 10,000 per reciprocal atom for ordered structures, and at least 5,000 for SQS structures employing the Monkhorst-Pack scheme.³⁹ The

energy cutoff of the wave function is taken as 350 eV, which is 1.3 times higher than the highest default value. The energy convergence criterion of the electronic self-consistency is chosen as 10^{-7} eV per atom for all the calculations. The reciprocal-space energy integration is performed by the Methfessel-Paxton technique⁴⁰ for structure relaxations. For the final calculations of total energies, electronic densities of state (DOS's), and stresses, we adopt the tetrahedron method incorporating a Blöchl correction.⁴¹ Due to the ferromagnetic (FM) nature of Ni, all the calculations are performed within the spin-polarized approximation except for fcc Pt. For the purpose of test, first-principles calculations are also performed for nonmagnetic (NM) structures of entries 1-29 (see Appendix).

The phonon calculations are performed by the supercell method⁴² as implemented in the ATAT code,⁴³ with VASP used as the computational engine. In the present work, supercells with at least 32 atoms are used, and displacements of 0.1 Å are adopted for the independent atoms in the perturbed supercells. In the VASP calculations, we use at least 2,000 k points per reciprocal atom and the Methfessel-Paxton technique⁴⁰ to calculate the forces acting on the atoms in the perturbed supercells. After the VASP calculations are complete, at least 4 Å is used as the cutoff range to fit the force constants and to get the phonon results by using ATAT. For more details of phonon calculations using the supercell method, see e.g. Refs. 44-46.

In order to fit the first-principles calculated energy vs. volume (E - V) data points, we use the four-parameter Birch-Murnaghan equation of state (EOS) in its linear form given by,⁴⁶

$$\text{Eq. 2} \quad E(V) = a + bV^{-2/3} + cV^{-4/3} + dV^{-2}$$

where a , b , c , and d are fitting parameters. The equilibrium properties estimated from this EOS include the volume (V_0), energy (E_0), bulk modulus (B_0) and its pressure derivative (B_0').⁴⁶ Conversely, based on the fitted equilibrium properties, the fitting parameters can be determined easily.⁴⁶ In the present work, usually six data points are used for the EOS fitting of each structure.

In order to estimate the finite temperature thermodynamic properties of a given phase of interest, we use the first-principles quasiharmonic approach to describe the Helmholtz free energy $F(V, T)$ at volume V and temperature T ,⁴⁵⁻⁴⁷

$$\text{Eq. 3} \quad F(V, T) = E(V) + F_{ele}(V, T) + F_{vib}(V, T)$$

where $E(V)$ is the static energy at 0 K without the zero-point vibrational energy, i.e., Eq. 2. $F_{ele}(V, T)$ represents the thermal electronic contribution at V and T , which is particularly important for metal systems due to the non-zero electronic density at the Fermi level. $F_{vib}(V, T)$ is the vibrational contribution determined by phonon calculations in the present work. For more details of the first-principles quasiharmonic approach, see e.g. Refs. 45-47.

III. RESULTS AND DISCUSSIONS

In this Section, we show firstly the reasons to choose the GGA potential instead of the LDA potential, and then the predicted properties for the disordered $\text{Ni}_{1-x}\text{Pt}_x$, including the bond length distributions and elastic constants (see Sec. III A), the equilibrium properties calculated by EOS fittings for both ordered and disordered $\text{Ni}_{1-x}\text{Pt}_x$ (see Sec. III B), and the predicted phase transition temperature between the ordered $L1_0$ structure and the disordered $\text{Ni}_{0.5}\text{Pt}_{0.5}$ (see Sec. III C). Note that without special mention, the present work discusses only the properties of FM $\text{Ni}_{1-x}\text{Pt}_x$ alloys.

Table 2 summarizes the EOS predicted lattice parameters and bulk moduli for fcc Ni and fcc Pt in comparison with experiments.⁴⁸⁻⁵⁰ Clearly, the GGA (rather than LDA) describes the fcc Ni very well, but the LDA (instead of GGA) is better for describing fcc Pt albeit the LDA is still not a good choice for Pt. The GGA potential is selected since the main focus of the present work is Ni and Ni based alloys.

A. Disordered Ni_{1-x}Pt_x: Bond length distributions and elastic properties

Since an SQS is an ordered structure with low symmetry (usually a monoclinic structure) designed to mimic the corresponding disordered structure, the relaxation of an SQS makes its cell shape and atomic positions deviate locally the ideal lattice. In order to examine the deviations of SQS's from the ideal fcc structure (taking Ni_{0.5}Pt_{0.5} as example), Fig. 1 plots the average radial distribution functions (RDF's) for the fully relaxed SQS's in comparison with the RDF of a pristine fcc structure, where the lattice parameter of the pristine fcc structure is calculated based on the average volume of SQS-8, SQS-16, and SQS-32. The RDF, used commonly to depict the liquid structure,⁵¹ describes how, on average, the atoms in a system are radially packed around each other. The RDF is defined by,

$$\text{Eq. 4} \quad g(r) = n(r) / (\rho 4\pi r^2 \Delta r)$$

where $n(r)$ is the mean number of atoms in a shell of width Δr at distance r , and ρ the average density of atoms in the system. Fig. 1 shows that the RDF's of SQS's, especially the ones of SQS-16 and SQS-32, are similar with the normal fcc case, indicating the fully relaxed SQS's for Ni_{0.5}Pt_{0.5} accurately represent fcc-like structures.

In order to probe the fluctuations of atomic positions in the disordered $\text{Ni}_{1-x}\text{Pt}_x$ alloys, Fig. 2 illustrates the bond length distributions in the first nearest neighbor region ($2.7 \pm 0.3 \text{ \AA}$) predicted by SQS's with compositions $x = 0.25, 0.5, \text{ and } 0.75$. Concerning the bond length distributions, there are no significant differences between SQS-8, SQS-16, and SQS-32, and a deviation up to 0.25 \AA away from the average bond length is shown for the disordered $\text{Ni}_{1-x}\text{Pt}_x$ alloys. With increasing Pt content, the average bond length increases due to Pt being a larger atom (see Table 2). Within each SQS structure, the bond lengths of Ni-Ni, Ni-Pt, and Pt-Pt are distinctly different. Most of the SQS's show that the Pt-Pt possesses largest average bond length, whereas the Ni-Ni has the smallest one, and the bond length of Ni-Pt is closer to Ni-Ni (the results from SQS-32's are shown in Fig. 2). It should be mentioned that the distinct bond length distributions are given by the SQS-32's instead of the SQS-16's and especially the SQS-8's.

The RDF's and the bond length distributions mostly give local information of the disordered alloys. In an effort to test the capability of SQS's to predict the global properties, we calculate the elastic stiffness constants (c_{ij} 's) by using an efficient first-principles strain-stress method with strains of ± 0.01 (see details in Refs. 49, 52-53). Table 3 shows that the predicted c_{ij} 's of $\text{Ni}_{0.5}\text{Pt}_{0.5}$ from the SQS-8, SQS-16, and SQS-32 structures. The following mean values of the c_{ij} 's are reported: (i) c_{11} from the average of $c_{11}, c_{22}, \text{ and } c_{33}$, (ii) c_{44} from the average of $c_{44}, c_{55}, \text{ and } c_{66}$, and (iii) c_{12} from the average of c_{ij} 's with $i \neq j$, and $i, j = 1, 2, \text{ and } 3$. The uncertainties, defined as the fluctuations of c_{ij} 's, are also given in Table 3 based on the calculations of the average c_{ij} 's. It is found that c_{11} has the largest uncertainty with respect to c_{12} and c_{44} , especially for SQS-8. In comparison with the c_{ij} 's obtained from fcc Ni and fcc Pt according to Vegard's law (the predicted c_{ij} 's of the pure elements were reported in Ref. 49), the calculated c_{11} directly from

SQS's for the disordered $\text{Ni}_{0.5}\text{Pt}_{0.5}$ is similar with the one from the Vegard's law. On the other hand, $c_{12}(\text{SQS}) < c_{12}(\text{Vegard})$, and $c_{44}(\text{SQS}) > c_{44}(\text{Vegard})$, with the differences around 10 GPa. The relationships between the aggregate properties of bulk modulus (B) and shear modulus (G) predicted from Voigt's approach and c_{ij} 's are found to be $B_{\text{Voigt}} < B_{\text{Vegard}}$ and $G_{\text{Voigt}} > G_{\text{Vegard}}$. The predicted B_{Voigt} 's are slightly larger by $\sim 1\text{-}4$ GPa than the B_{EOS} 's from EOS fittings, agreeing with the previous observations for these two kinds of methods (c_{ij} 's vs. EOS)⁵² and the trend is due to the cell shape relaxations included in the EOS fitting but not in the determinations of the c_{ij} 's. Based on the above analysis, we conclude that the SQS's can be used to predict the elastic properties of the disordered alloys, and the uncertainties for the predicted elastic properties can be estimated.

B. Equilibrium properties from EOS fittings

Based on the ordered and disordered structures shown in the Appendix, the EOS (using Eq. 2) fitted properties for FM $\text{Ni}_{1-x}\text{Pt}_x$ are shown in Table 4, including V_0 , B_0 , B_0' , ΔE_0 (i.e., the relative enthalpy ΔH_0 due to the zero external pressure used herein), and the magnetic moment (MM_0).

In Table 4, we also list the experimental data^{7, 17, 54-55} when available, and the pair correction functions for the disordered and ordered structures up to the fourth nearest neighbor. For the convenience of discussion, we plot these properties of FM alloys as a function of Pt content in Fig. 3. With increasing Pt concentration, Fig. 3 shows that both the equilibrium volume and the equilibrium bulk modulus increase. The variation of bulk modulus vs. volume is opposite to the common observation, i.e. the larger the volume the smaller the bulk modulus,⁴⁹ due to the large volume and large bulk modulus of fcc Pt with respect to those of fcc Ni (see Table 2). From Fig. 3, we find that the variation of volume shows a slight positive deviation from Vegard's law for

$\text{Ni}_{1-x}\text{Pt}_x$ (e.g., the deviations of $0.13 \sim 0.37 \text{ \AA}^3/\text{atom}$ for $\text{Ni}_{0.5}\text{Pt}_{0.5}$), and correspondingly, a negative deviation is predicted for the change of bulk modulus (e.g., the deviations of $-5.3 \sim -10.2 \text{ GPa}$ for $\text{Ni}_{0.5}\text{Pt}_{0.5}$). Fig. 4 shows the variations of the derivative of bulk modulus relative to pressure (B_0') and the magnetic moment (MM_0) for $\text{Ni}_{1-x}\text{Pt}_x$. With increasing Pt content, B_0' increases roughly linearly in the range of $4.9 \sim 5.5$, whereas the MM_0 decreases with a shallower slope than experimental measurements,⁵⁴ but agrees with previous first-principles predictions.⁵⁶ Regarding the values of V_0 , B_0 , B_0' , and MM_0 of the SQS's, the properties are roughly located in the middle of the results for ordered structures (see Fig. 3 and Fig. 4).

Fig. 5 shows the first-principles calculated relative energies of the ordered compounds and disordered (i.e., SQS's) $\text{Ni}_{1-x}\text{Pt}_x$ alloys at 0 K in comparison with the experimental data at room temperature,⁵⁵ with the reference states of fcc Ni and fcc Pt. The CEM predicted curve for the disordered phases are based on the results of ordered structures, and the predicted curve for the disordered phases by Redlich-Kister (R-K)⁵⁷ polynomial are based on the SQS results. Regarding the CEM predictions, 34 distinct ECI's according to cross-validation¹⁵ are used, including the constant and point terms that have no effect on the results, 25 pair interactions, and 7 triplet terms. The R-K polynomial, commonly used in the CALPHAD modeling,⁵⁸ is given by,

$$\text{Eq. 5} \quad E(x) = x_i x_j (L_0 + L_1 (x_i - x_j))$$

where x_i is the mole fraction of Pt, and $x_j = 1 - x_i$ the mole fraction of Ni. The two-parameter form (L_0 and L_1) is adopted in the present work with the fitted $L_0 = -185.09$ and $L_1 = 23.56$ in units of meV/atom. When $x = 0.25$, Fig. 5 shows that the ground state of Ni_3Pt at 0 K is the ferromagnetic phase with D0_{22} structure instead of the common belief of L1_2 structure (see the detailed analysis in Ref. 59). Regarding the CEM predicted adaptive crystal structure (ACS) of

NiPt₇ by Sanati et al.,²⁹ our calculation shows that its formation energy with respect to L1₂-NiPt₃ and fcc Pt is almost zero, indicating ACS-NiPt₇ is not an energetically favorable structure, in agreement with first-principles predictions and experimental measurements by Schonfeld et al.⁶⁰ In the lower Pt region, the formation energies are scattered and some structures have higher energies, e.g., α_1 , V_1 , and Z_1 structures, making the CEM predicted energies for the disordered phases less accurate due to the truncated errors when determining ECI's, and they are also higher than the predictions by the R-K polynomial. For instance, Fig. 5 indicates the CEM predicted energy are quite high for fcc Ni due to the truncated errors especially in the lower Pt region. The truncated error is one of the major issues of CEM, we therefore believe more the SQS predictions instead of CEM results for disordered phase, at least for the present Ni_{1-x}Pt_x alloys. For the SQS predicted energies, the results are close to each other for SQS-16's and SQS-32's, but the result of SQS-8 is deviates from the results of SQS-16, SQS-32, the CEM predictions, and the R-K polynomial approximation. Note that there are nine 8-atom structures with pair correction functions for the first and the second nearest neighbors that match the disordered case, and in the present work we pick one of them as SQS-8 based on the pair correction function of the third nearest neighbor (see Table 1). The calculated relative energies for these 9 structures locate in a large range of -62 to -27 meV/atom. Based on the results shown in Fig. 5 and also Fig. 1, we conclude that SQS-8 is less accurate to describe the energy of the disordered phase in comparison with SQS-16 and SQS-32. In principle, Fig. 5 also shows that the closer the correction functions to the disordered phase, the closer their energies relative to the disordered phases (e.g., β_1 and Y_2 structure), but we also find an exception with β_2 (see Fig. 5 and Table 4). In addition, good agreement is also found between the predicted ground state line and the experimental data.⁵⁵

As ancillary tests, the EOS fitted properties (V_0 , B_0 , B_0' , and ΔE_0) for NM $\text{Ni}_{1-x}\text{Pt}_x$ are also shown for entries 1-29 in Table 4. As expected, the NM phases of $\text{Ni}_{1-x}\text{Pt}_x$ have higher energies relative to the corresponding FM $\text{Ni}_{1-x}\text{Pt}_x$ with the differences of 7~54 meV/atom, indicating the FM states are ground states for $\text{Ni}_{1-x}\text{Pt}_x$. Therefore, the results of FM $\text{Ni}_{1-x}\text{Pt}_x$ are presented mainly and discussed in the present work. Regarding the equilibrium volumes of $\text{Ni}_{1-x}\text{Pt}_x$, the NM states possess smaller values in comparison with the corresponding FM ones with the differences around $0.1 \text{ \AA}^3/\text{atom}$ due to the effect of magnetism. Accordingly, the NM states of $\text{Ni}_{1-x}\text{Pt}_x$ have larger bulk moduli with respect to the corresponding FM states. It is worth mentioning that the present predictions of V_0 , B_0 , and ΔE_0 are in perfect agreement with the previous first-principles results, e.g., the work of Che et al.,⁶¹ for both FM and NM $\text{Ni}_{1-x}\text{Pt}_x$. For example, the ΔE_0 's of Ni_3Pt (FM, $L1_2$), NiPt ($L1_0$, FM), and NiPt_3 (FM, $L1_2$) are -69, -93, and -64 meV/atom, respectively (see Table 4), correspondingly the values from Che et al.⁶¹ are -71, -92, and -65 meV/atom, respectively.

C. Phonon and finite temperature thermodynamics

In the present work, we calculate the phonon properties for all the structures listed in the Appendix of $\text{Ni}_{0.5}\text{Pt}_{0.5}$. As examples, Fig. 6 illustrates the phonon DOS's for three low energy structures of $L1_0$, "40", and W_2 , and two SQS structures of SQS-8 and SQS-16, as well as the generalized phonon DOS (GDOS) derived from incoherent inelastic scattering.⁶² Note that (i) all the phonon DOS's have the same integral values compared to each other, and (ii) the experimental GDOS is only shown for reference, since there exists big difference between the normal phonon DOS and the GDOS. Here, the GDOS can be represented by

$$\text{GDOS} = \sum_i (\sigma_i / M_i) \text{pDOS}_i$$
,
 where σ_i , M_i , and pDOS_i are the atomic scattering cross section, the atomic mass, and the partial phonon DOS of atom i , respectively.⁶³ The normal phonon DOS's are presented in this work, since they can be used directly to predict thermodynamic properties. Fig. 6 indicates that the maximum frequencies from the predictions in this work are less than the measured one due to the fact that the GGA predicts weaker bonding than reality which is represented through a smaller bulk modulus (see Table 2). In general, the ordered structures have sharper peaks than the disordered ones (SQS's), indicating that the disordered phonon DOS's are similar to those of the ordered cases but with more spread in their peaks, agreeing roughly with the measured shape in high frequency region (see Fig. 6). To gain insight into the bonding nature of $\text{Ni}_{0.5}\text{Pt}_{0.5}$, Fig. 7 shows the stretching and bending force constants for all the structures at their equilibrium volumes (see Table 4), together with the force constants of fcc Ni and fcc Pt for comparison. It is found that all the $\text{Ni}_{0.5}\text{Pt}_{0.5}$ structures are stable or metastable ones except for the $L1_1$ structure due to its negative force constants in the second and especially third nearest neighbor regions (the structure instability caused by the negative force constants was reported in e.g. Refs. 44, 64-65). In general, the force constants for all the structures examined herein, including the pure elements, possess a similar regularity of bond length vs. bond stiffness. Fig. 7 indicates that the bonds in order of decreasing strength are the Pt-Pt, the Ni-Pt, and finally the Ni-Ni atomic pairs for both the ordered and disordered alloys. The main contributions of force constants are the ones in the first-nearest neighbor region ($2.7 \pm 0.3 \text{ \AA}$), with the exception being the unstable $L1_1$ structure.

As an application of the phonon DOS's, the Helmholtz free energies of the L1₀ and SQS-16 structures are predicted for Ni_{0.5}Pt_{0.5} by using the quasiharmonic approach described in Eq. 3. In Fig. 8, we plot the relative thermodynamics properties of SQS-16 under external pressure $P = 0$ with the L1₀ structure as the reference state. Regarding the configurational entropy of the disordered phase, we use the point approximation, also known as the Bragg-Williams approximation,⁶⁶

$$\text{Eq. 6} \quad S_{\text{conf}}(x) = -k_B [x \log x + (1-x) \log(1-x)]$$

where x is the mole fraction of Pt, and k_B the Boltzmann constant. With the contribution of only the relative vibrational entropy (ΔS_{vib}), the relative Helmholtz free energy (ΔF) decreases slowly due to the small contribution from ΔS_{vib} (around $0.13 k_B$ per atom from 200 ~ 1000 K). Note that the presently predicted ΔS_{vib} of NiPt agrees well with the value between the ordered and disordered CuAu.⁶⁷ With the contribution of only the relative configurational entropy (ΔS_{conf}), ΔF decreases more quickly, resulting in a phase transition temperature of 905 K, that agrees with the experimental value around 900 K (the reported temperatures are 876 and 918 K with the latter one being more accurate⁷). With the contributions of both ΔS_{vib} and ΔS_{conf} , the predicted phase transition temperature is 755 K, which is much lower than the experimental value. It should be mentioned that the predicted order-disorder phase transition temperature is sensitive to the energy difference at 0 K. Table 4 (see also Fig. 5) shows that the relative energy (ΔE) of Ni_{0.5}Pt_{0.5} between L1₀ and SQS-16 structures is 54.1 meV/atom without the zero-point vibrational energy. From consideration of the predicted ΔE 's of SQS-8 and SQS-32, the energy uncertainty is estimated to be ± 9.15 meV/atom, resulting in an uncertainty of ± 128 K for the phase transition temperature. Therefore, the predicted phase transition temperature between L1₀

and the disordered $\text{Ni}_{0.5}\text{Pt}_{0.5}$ is 755 ± 128 K with considerations from ΔS_{vib} and ΔS_{conf} . The temperature agrees reasonably well with the experimental value around 900 K,⁷ wherein the driving force of phase transition is mainly due to the configurational entropy instead of the vibrational entropy. It is worth mentioning that the less accurate phase transition temperature predicted in the present work may be related to (i) the less accurate density functional theory, especially the exchange-correlation functional for Pt (see Table 2), and (ii) the omission of magnetic phase transition in $\text{Ni}_{1-x}\text{Pt}_x$ alloys. We think the first is the major effect, while the latter is the minor one, because we treat both the $L1_0$ and SQS structures on an equal footing by using the FM structures, the magnetic contributions to thermodynamics for both ordered and disordered phases therefore can be cancelled to some extent. Regarding the longstanding issue of magnetic contribution to finite temperature thermodynamics, it is beyond the scope of the present work and has not been resolved completely, although we are on the way to the solution by using first-principles partition function method.^{14, 68-70} It is also worth mentioning that the high temperature paramagnetic (PM) phase is not the simple NM phase, instead, PM is a disordered FM phase with the zero total magnetic moment. For the sake of simplicity, the complete consideration of magnetic phase transition in each phase is omitted in the present work.

IV. CONCLUSIONS

By using the first-principles and phonon calculations, we study the structural, vibrational, and thermodynamic properties of the ordered and disordered $\text{Ni}_{1-x}\text{Pt}_x$ alloys with the main focus on the disordered $\text{Ni}_{0.5}\text{Pt}_{0.5}$. In order to describe the disordered alloys, special quasirandom structures (SQS's) are adopted, and we demonstrate their capabilities to predict local and global properties of disordered alloys including bond length distributions, phonon spectra, and elastic

stiffness constants. For both the ordered and disordered $\text{Ni}_{1-x}\text{Pt}_x$ alloys, it is found that (i) the Pt-Pt bond is stronger than the Ni-Pt and the Ni-Ni bonds according to the force constants; (ii) a slight positive deviation from Vegard's law is predicted for the volume variation of $\text{Ni}_{1-x}\text{Pt}_x$, and correspondingly, a negative deviation is obtained for the change of bulk modulus; (iii) with increasing Pt content, the derivative of bulk modulus relative to pressure increases roughly linearly, while the magnetic moment decreases. For the disordered $\text{Ni}_{1-x}\text{Pt}_x$ alloys, the analysis of the bond length distributions is more accurate with greater number of atoms in the SQS, particularly the SQS-32 case, the Pt-Pt atomic pairs possess the longest bond lengths relative to the Ni-Pt and Ni-Ni ones in the disordered alloys, and the phonon density of states of the disordered alloys are like broadened-peak versions of the ordered cases. In addition, the SQS predicted enthalpies of formation (relative energies) for the disordered $\text{Ni}_{1-x}\text{Pt}_x$ are also compared with the predicted relative energies by the cluster expansion method. As an application of the finite temperature thermodynamic properties, the phase transition temperature is predicted to be 755 ± 128 K between the ordered $L1_0$ and the disordered $\text{Ni}_{0.5}\text{Pt}_{0.5}$. The predicted transition temperature agrees reasonably well with the measurement around 900 K, and the driving force of phase transition is mainly due to the configurational entropy instead of the vibrational entropy.

ACKNOWLEDGEMENTS

This work was funded by the Office of Naval Research (ONR) under contract No. N0014-07-1-0638 and the National Science Foundation (NSF) through Grant No. DMR-1006557. First-principles calculations were carried out partially on the LION clusters supported by the Materials Simulation Center and the Research Computing and Cyber infrastructure unit at Pennsylvania

State University, and partially on the resources of NERSC supported by the Office of Science of the U. S. DOE under contract No. DE-AC02-05CH11231.

APPENDIX

See Table A1 and Table A2 for the fcc based ordered and disordered SQS structures used in the present work.

Table A1.

Structural details for all independent, fcc based A_mB_n structures with $m, n = 0, 1, \dots, 4$, and $m+n \leq 4$ (entries 1-29) and a few fcc based structures with $8 \geq m+n \geq 5$ (entries 30-37), where (i) the lattice parameter of fcc structure is set as unity, (ii) "Name" indicates the Strukturbericht designation or the commonly used one in the literature,²⁹⁻³¹ and (iii) "SG" represents the space group.

Entry	Formula	Name	SG	Primitive vectors	Atoms	Atomic/Wyckoff sites
1 (2)	A (B)	A1	$Fm\bar{3}m$ (#225)	(0, 1/2, 1/2) (1/2, 0, 1/2) (1/2, 1/2, 0)	A ^a (4a) ^b	(0, 0, 0)
3	AB	L1 ₁	$R\bar{3}m$ (#166)	(1, 1/2, 1/2) (1/2, 1, 1/2) (1/2, 1/2, 1)	A (1a) B (1b)	(0, 0, 0) (1/2, 1/2, 1/2)
4	AB	L1 ₀	$P4/mmm$ (#123)	(1/2, -1/2, 0) (1/2, 1/2, 0) (0, 0, 1)	A (1a) B (1d)	(0, 0, 0) (1/2, 1/2, 1/2)
5 (6)	A ₂ B (AB ₂)	α_1 (α_2)	$P\bar{3}m1$ (#164)	(-1/2, 0, -1/2) (0, -1/2, 1/2) (-1, 1, 1)	A (1a) B (2d)	(0, 0, 0) (1/3, 2/3, 1/3); (2/3, 1/3, 2/3)
7 (8)	A ₂ B (AB ₂)	γ_1 (γ_2)	$Immm$ (#71)	(-1/2, 1/2, -1) (-1, -1/2, -1/2) (1/2, 1/2, 1)	A (2a) B (4g)	(0, 0, 0) (1/3, 1/3, 0); (2/3, 2/3, 0)
9 (10)	A ₂ B (AB ₂)	β_1 (β_2)	$I4/mmm$ (#139)	(0, -1/2, -3/2) (0, 1/2, -3/2) (1/2, 0, 3/2)	A (2a) B (4e)	(0, 0, 0) (1/3, 1/3, 0); (2/3, 2/3, 0)
11 (13)	A ₃ B (AB ₃)	V ₁ (V ₃)	$R\bar{3}m$ (#166)	(-3/2, 1, 3/2) (-1, 3/2, 3/2) (-3/2, 3/2, 1)	A (1a) B (1b) B (2c)	(0, 0, 0) (1/2, 1/2, 1/2) (1/4, 1/4, 1/4); (3/4, 3/4, 3/4)
12	A ₂ B ₂	V ₂			A (2c) B (2c)	(0, 0, 0); (1/4, 1/4, 1/4) (1/2, 1/2, 1/2); (3/4, 3/4, 3/4)
14 (16)	A ₃ B (AB ₃)	W ₁ (W ₃)	$C2/m$ (#12)	(-1, -1/2, -1/2) (-1/2, -1/2, -1) (1/2, -1, 1/2)	A (2a) B (2d) B (4i)	(0, 0, 0) (1/2, 1/2, 1/2) (1/4, 1/4, 3/4); (3/4, 3/4, 1/4)
15	A ₂ B ₂	W ₂			A (4i) B (4i)	(0, 0, 0); (1/4, 1/4, 3/4) (1/2, 1/2, 1/2); (3/4, 3/4, 1/4)
17 (18)	A ₃ B (AB ₃)	L1 ₃	$Cmmm$ (#65)	(1, 1/2, 1/2) (-1, 1/2, 1/2) (0, -1/2, 1/2)	A (2a) B (2b) B (4f)	(0, 0, 0) (1/2, 1/2, 0) (1/2, 0, 1/2) (0, 1/2, 1/2)
19 (21)	A ₃ B (AB ₃)	D0 ₂₂	$I4/mmm$ (#139)	(-1, -1/2, 1/2) (-1, 1/2, -1/2) (1, -1/2, -1/2)	A (2a) B (2b) B (4d)	(0, 0, 0) (1/2, 1/2, 0) (1/4, 3/4, 1/2); (3/4, 1/4, 1/2)
20	A ₂ B ₂	40	$I41/amd$		A (4a) B (4b)	(0, 0, 0); (1/4, 3/4, 1/2) (1/2, 1/2, 0); (3/4, 1/4, 1/2)

(#141)						
22 (24)	A ₃ B (AB ₃)	Y ₁ (Y ₃)	<i>Pmmm</i> (#47)	(0, -1/2, -1/2) (-1, 0, 0) (0, 1, -1)	A (1a) B (1c) B (2t)	(0, 0, 0) (0, 0, 1/2) (1/2, 1/2, 1/4); (1/2, 1/2, 3/4)
23	A ₂ B ₂	Y ₂	<i>Pmmn</i> (#59)		A (2a) B (2a)	(0, 0, 0); (1/2, 1/2, 1/4) (0, 0, 1/2); (1/2, 1/2, 3/4)
25 (27)	A ₃ B (AB ₃)	Z ₁ (Z ₃)	<i>P4/mmm</i> (#123)	(-1/2, -1/2, 0) (1/2, -1/2, 0) (0, 0, 2)	A (1a) B (1b) B (2h)	(0, 0, 0) (0, 0, 1/2) (1/2, 1/2, 1/4); (1/2, 1/2, 3/4)
26	A ₂ B ₂	Z ₂	<i>P4/nmm</i> (#129)		A (2c) B (2c)	(0, 0, 0); (1/2, 1/2, 1/4) (0, 0, 1/2); (1/2, 1/2, 3/4)
28 (29)	A ₃ B (AB ₃)	L1 ₂	<i>Pm$\bar{3}$m</i> (#221)	(1, 0, 0) (0, 1, 0) (0, 0, 1)	A (1a) B (3c)	(0, 0, 0) (1/2, 1/2, 0); (1/2, 0, 1/2) (0, 1/2, 1/2)
30 (31)	A ₄ B (AB ₄)	mC10 ^c	<i>C2/m</i> (#12)	(3/2, 0, -1/2) (3/2, 1/2, 0) (-1, -1, 1)	A (2a) B (4i) B (4i)	(0, 0, 0) (1/5, 1/5, 3/5); (4/5, 4/5, 2/5) (2/5, 2/5, 1/5); (3/5, 3/5, 4/5)
32 (33)	A ₄ B (AB ₄)	D1 _a	<i>I4/m</i> (#87)	(-1/2, -1, 1/2) (1/2, 1, 1/2) (-1, 1/2, -1/2)	A (2a) B (8h)	(0, 0, 0) (1/5, 2/5, 3/5); (4/5, 3/5, 2/5) (3/5, 1/5, 4/5); (2/5, 4/5, 1/5)
34 (35)	A ₇ B (AB ₇)	D1 (D7)	<i>Fm$\bar{3}$m</i> (#225)	(0, 1, 1) (1, 0, 1) (1, 1, 0)	A (4a) B (4b) B (24d)	(0, 0, 0) (1/2, 1/2, 1/2) (1/2, 0, 0); (0, 1/2, 0) (0, 0, 1/2); (1/2, 1/2, 0) (1/2, 0, 1/2); (0, 1/2, 1/2)
36 (37)	A ₇ B (AB ₇)	ACS ^d	<i>I4/mmm</i> (#139)	(-2, -1/2, 1/2) (-2, 1/2, -1/2) (2, -1/2, -1/2)	A (2a) B (2b) B (4e) B (8g)	(0, 0, 0) (1/2, 1/2, 0) (1/4, 1/4, 0); (3/4, 3/4, 0) (1/8, 5/8, 1/2); (3/8, 7/8, 1/2) (5/8, 1/8, 1/2); (7/8, 3/8, 1/2)

^a Atoms are given for one of the structures.

^b Wyckoff letter with multiplicity.

^c Pearson symbol.

^d Reference 29.

Table A2

Lattice vectors and atomic positions (fractional coordinates) for fcc based SQS structures with 8, 16, and 32 atoms. Note that (i) the lattice parameter of fcc structure is set as unity, (ii) all the available structures are tested by using the ATAT code improved by the present author YW.²⁸

<p>SQS-8 (A_4B_4)^a Lattice vectors: (1, 1/2, -1/2) (1/2, 1/2, -1) (-1, 2, 1) A atoms: (0, 0, 1/2); (1/2, 1/2, 1/4) (3/4, 3/4, 5/8); (3/4, 3/4, 1/8) B atoms: (0, 0, 0); (1/4, 1/4, 7/8) (1/4, 1/4, 3/8); (1/2, 1/2, 3/4)</p>	<p>SQS-8 (A_2B_6)^a Lattice vectors: (1/2, -1, -1/2) (1/2, -1, 1/2) (-2, 0, 0) A atoms: (0, 0, 0); (3/4, 3/4, 1/8) B atoms: (1/4, 1/4, 7/8); (1/2, 1/2, 3/4); (3/4, 3/4, 5/8) (0, 0, 1/2); (1/4, 1/4, 3/8); (1/2, 1/2, 1/4)</p>
<p>SQS-16 (A_8B_8)^b Lattice vectors: (1, -1/2, -1/2) (0, 1, -1) (1, 3/2, 3/2) A atoms: (1/4, 1/4, 1/4); (1/4, 3/4, 1/4) (3/4, 1/2, 1/4); (1/4, 0, 3/4); (0, 1/4, 1/2) (1/2, 3/4, 0); (0, 1/2, 0); (0, 0, 0) B atoms: (1/2, 1/2, 1/2); (3/4, 0, 1/4) (1/2, 0, 1/2); (1/4, 1/2, 3/4); (0, 3/4, 1/2) (3/4, 1/4, 3/4); (3/4, 3/4, 3/4); (1/2, 1/4, 0)</p>	<p>SQS-16 (A_4B_{12})^b Lattice vectors: (1/2, 1/2, -1) (0, -3/2, -1/2) (-2, 1/2, -1/2) A atoms: (3/4, 5/16, 3/16); (1/4, 7/16, 1/16) (0, 3/4, 1/4); (3/4, 1/16, 7/16) B atoms: (1/2, 7/8, 1/8); (1/4, 3/16, 5/16) (0, 1/2, 1/2); (1/2, 5/8, 3/8); (1/2, 3/8, 5/8) (1/4, 11/16, 13/16); (0, 0, 0); (0, 1/4, 3/4) (1/4, 15/16, 9/16); (3/4, 9/16, 15/16) (1/2, 1/8, 7/8); (3/4, 13/16, 11/16)</p>
<p>SQS-32 ($A_{16}B_{16}$)^c Lattice vectors: (0, 1, -3) (-1, -5/2, 3/2) (0, 3, -1) A atoms: (1/16, 1/2, 1/16); (3/16, 1/2, 3/16) (5/8, 0, 1/8); (1/16, 1/2, 9/16); (0, 0, 0) (11/16, 1/2, 3/16); (9/16, 1/2, 1/16) (7/16, 1/2, 7/16); (13/16, 1/2, 5/16); (1/2, 0, 0) (9/16, 1/2, 9/16); (5/16, 1/2, 13/16); (1/4, 0, 1/4) (15/16, 1/2, 7/16); (1/8, 0, 5/8); (3/4, 0, 1/4) B atoms: (3/16, 1/2, 11/16); (5/8, 0, 5/8) (5/16, 1/2, 5/16); (0, 0, 1/2); (7/8, 0, 7/8) (1/8, 0, 1/8); (11/16, 1/2, 11/16); (3/4, 0, 3/4) (3/8, 0, 3/8); (13/16, 1/2, 13/16); (1/2, 0, 1/2) (1/4, 0, 3/4); (15/16, 1/2, 15/16); (7/8, 0, 3/8) (3/8, 0, 7/8); (7/16, 1/2, 15/16)</p>	<p>SQS-32 (A_8B_{24})^c Lattice vectors: (0, -1, -1) (-2, 0, 0) (0, 2, -2) A atoms: (1/2, 1/2, 1/2); (1/4, 3/4, 3/8) (1/4, 3/4, 1/8); (0, 1/2, 1/4); (1/2, 0, 1/4) (1/4, 1/4, 1/8); (1/2, 0, 0); (3/4, 3/4, 5/8) B atoms: (0, 0, 0); (0, 1/2, 0); (0, 1/2, 1/2) (3/4, 3/4, 1/8); (1/2, 1/2, 0); (1/4, 3/4, 5/8) (3/4, 3/4, 3/8); (1/2, 1/2, 1/4); (0, 0, 3/4) (3/4, 1/4, 3/8); (1/4, 1/4, 3/8); (0, 0, 1/4) (3/4, 3/4, 7/8); (1/4, 3/4, 7/8); (0, 0, 1/2) (0, 1/2, 3/4); (3/4, 1/4, 5/8); (1/4, 1/4, 5/8) (1/2, 0, 1/2); (3/4, 1/4, 7/8); (1/2, 1/2, 3/4) (1/4, 1/4, 7/8); (1/2, 0, 3/4); (3/4, 1/4, 1/8)</p>

^a See also the SQS-8's reported in Refs. 20-21.

^b The same as the ones reported in Ref. 26.

^c The present work.

Tables and Table captions

Table 1. Pair correction functions $\Pi_{2,n}$ (n up to the 11th nearest neighbor) for the random (disordered) structures and the fcc based SQS structures (see Appendix for the structure details).

Structure	$\Pi_{2,1}$	$\Pi_{2,2}$	$\Pi_{2,3}$	$\Pi_{2,4}$	$\Pi_{2,5}$	$\Pi_{2,6}$	$\Pi_{2,7}$	$\Pi_{2,8}$	$\Pi_{2,9}$	$\Pi_{2,10}$	$\Pi_{2,11}$
Random ($A_{0.5}B_{0.5}$)	0	0	0	0	0	0	0	0	0	0	0
SQS-8 (A_4B_4)	0	0	1/24	-1/12	1/12	0	-1/8	-1/2	1/12	0	0
SQS-16 (A_8B_8)	0	0	0	0	0	0	0	-1	0	0	0
SQS-32 ($A_{16}B_{16}$)	0	0	0	0	0	0	0	0	-1/12	-1/6	0
Random ($A_{0.25}B_{0.75}$)	1/4	1/4	1/4	1/4	1/4	1/4	1/4	1/4	1/4	1/4	1/4
SQS-8 (A_2B_6)	1/4	1/3	1/4	0	1/6	0	1/3	2/3	1/4	1/12	1/3
SQS-16 (A_4B_{12})	1/4	1/4	1/4	5/24	11/48	1/8	19/96	1/4	19/48	1/4	1/6
SQS-32 (A_8B_{24})	1/4	1/4	1/4	1/4	1/4	1/4	1/4	1/3	1/6	1/6	1/4

Table 2. First-principles EOS calculated lattice parameters and bulk moduli of fcc Ni and fcc Pt by GGA and LDA, where the percent errors between the predictions and the experiments are shown in the parentheses.

Element	Lattice parameter (\AA) and error			Bulk modulus (GPa) and error		
	GGA	LDA	Expt. ^a	GGA	LDA	Expt. ^b
fcc Ni	3.521 (0.1%)	3.425 (-2.8%)	3.525	195.7 (4.7%)	255.6 (-36.7%)	187
fcc Pt	3.986 (1.6%)	3.907 (-0.4%)	3.922	242.9 (15.7%)	304.7 (-5.8%)	288

^a References 48-49.

^b References 49-50.

Table 3. First-principles calculated elastic properties (GPa) for the disordered $Ni_{0.5}Pt_{0.5}$, including the elastic constants (c_{ij} 's), bulk modulus (B_{Voigt} approach from c_{ij} 's and B_{EOS} from EOS fitting), and shear modulus (G_{Voigt}).

Structure	c_{11}	c_{12}	c_{44}	B_{Voigt}	B_{EOS}	G_{Voigt}
SQS-8	280 ± 26	179 ± 2	102 ± 2	213 ± 10	211	82 ± 6
SQS-16	287 ± 14	181 ± 1	101 ± 3	216 ± 5	212	82 ± 4
SQS-32	279 ± 14	183 ± 5	99 ± 3	215 ± 8	212	78 ± 3
(Ni+Pt)/2 ^a	286	193	89	224		72

^a Based on the predicted elastic constants of pure elements⁴⁹ and Vegard's law.

Table 4. Pair correction function ($\Pi_{2,rand}$) for the random (disordered) alloy, and the pair correction functions ($\Pi_{2,n}$) up to the fourth nearest neighbors for fcc based ordered structures (entries 1-37) and SQS structures (entries 38-46), together with the first-principles properties at 0 K fitted by Birch-Murnaghan EOS, including the equilibrium volume V_0 ($\text{\AA}^3/\text{atom}$), relative energy ΔE_0 (meV/atom) with the reference states of fcc Ni (FM state) and fcc Pt (NM state), bulk modulus B_0 (GPa) and its pressure derivative B_0' , and the magnetic moment MM_0 (μ_B/atom). As examples, calculated results for NM states are also shown for entries 1-29.

Entry ^a	Name ^a	Formula ^a	$\Pi_{2,rand}$	$\Pi_{2,1}$	$\Pi_{2,2}$	$\Pi_{2,3}$	$\Pi_{2,4}$	State	V_0	ΔE_0	B_0	B_0'	MM_0
1	A1	Ni	1	1	1	1	1	FM	10.92	0.0	195.7	4.95	0.61
								NM	10.85	54.3	199.7	4.95	
								FM	10.95 ^b		187 ^b		0.62 ^c
2	A1	Pt	1	1	1	1	NM	15.83	0.0	242.9	5.51	0.00	
							NM	15.08 ^b		288 ^b			
3	L1 ₁	NiPt	0	0	-1	0	1	FM	13.71	-52.9	213.3	5.22	0.51
								NM	13.61	-22.5	219.3	5.27	
4	L1 ₀	NiPt	0	-1/3	1	-1/3	1	FM	13.53	-93.3	213.3	5.24	0.51
								NM	13.42	-77.9	220.7	5.26	
								FM	13.46 ^d	-96 ^e			0.22 ^c
5	α_1	Ni ₂ Pt	1/9	1/3	-1/3	0	1/3	FM	12.94	3.5	205.7	5.16	0.54
								NM	12.84	43.3	210.5	5.17	
6	α_2	NiPt ₂	1/9	1/3	-1/3	0	1/3	FM	14.47	-46.3	218.7	5.32	0.48
								NM	14.37	-27.1	226.0	5.51	
7	γ_1	Ni ₂ Pt	1/9	-1/9	1/9	1/3	-1/9	FM	12.74	-68.8	205.6	5.14	0.57
								NM	12.64	-33.8	211.3	5.16	
8	γ_2	NiPt ₂	1/9	-1/9	1/9	1/3	-1/9	FM	14.41	-42.0	220.9	5.39	0.47
								NM	14.32	-29.3	226.0	5.36	
9	β_1	Ni ₂ Pt	1/9	1/9	5/9	-1/3	1/9	FM	12.73	-37.9	204.1	5.13	0.53
								NM	12.61	-12.5	210.7	5.14	
10	β_2	NiPt ₂	1/9	1/9	5/9	-1/3	1/9	FM	14.31	-72.4	222.2	5.34	0.47
								NM	14.21	-58.7	228.1	5.36	
11	V ₁	Ni ₃ Pt	1/4	1/2	0	1/4	1/2	FM	12.51	26.6	202.0	5.11	0.55
								NM	12.43	68.5	206.7	5.12	
12	V ₂	Ni ₂ Pt ₂	0	1/2	0	0	0	FM	13.74	3.2	211.4	5.22	0.48
								NM	13.65	30.2	217.3	5.31	
13	V ₃	NiPt ₃	1/4	1/2	0	1/4	1/2	FM	14.81	-32.7	222.9	5.51	0.37
								NM	14.74	-22.3	230.6	5.51	
14	W ₁	Ni ₃ Pt	1/4	1/6	0	1/4	1/2	FM	12.34	-42.6	202.4	5.11	0.56
								NM	12.25	-4.1	208.3	5.12	
15	W ₂	Ni ₂ Pt ₂	0	-1/6	0	0	0	FM	13.56	-67.7	209.1	5.31	0.53
								NM	13.45	-44.7	214.7	5.27	
16	W ₃	NiPt ₃	1/4	1/6	0	1/4	1/2	FM	14.81	-36.1	226.8	5.47	0.40
								NM	14.74	-23.8	230.8	5.41	
17	L1 ₃	Ni ₃ Pt	1/4	1/6	0	1/6	1	FM	12.38	-40.1	202.4	5.08	0.55
								NM	12.28	-4.9	209.2	5.12	

18	L1 ₃	NiPt ₃	1/4	1/6	0	1/6	1	FM	14.83	-46.7	227.2	5.41	0.36
								NM	14.77	-27.4	231.3	5.41	
19	D0 ₂₂	Ni ₃ Pt	1/4	0	2/3	1/3	1/3	FM	12.27	-71.6	203.6	5.06	0.59
								NM	12.18	-35.4	210.4	5.12	
20	“40”	Ni ₂ Pt ₂	0	-1/3	1/3	1/3	-1/3	FM	13.57	-71.3	214.0	5.25	0.53
								NM	13.48	-48.7	220.0	5.27	
21	D0 ₂₂	NiPt ₃	1/4	0	2/3	1/3	1/3	FM	14.76	-44.9	224.2	5.38	0.35
								NM	14.70	-38.4	231.8	5.43	
22	Y ₁	Ni ₃ Pt	1/4	1/6	1/3	1/6	1/3	FM	12.32	-40.2	202.2	5.08	0.58
								NM	12.22	-4.8	207.9	5.13	
23	Y ₂	Ni ₂ Pt ₂	0	0	-1/3	0	-1/3	FM	13.63	-46.9	212.5	5.27	0.54
								NM	13.53	-19.6	217.2	5.29	
24	Y ₃	NiPt ₃	1/4	1/6	1/3	1/6	1/3	FM	14.79	-30.1	221.0	5.21	0.39
								NM	14.72	-23.6	230.5	5.40	
25	Z ₁	Ni ₃ Pt	1/4	1/3	2/3	0	1/3	FM	12.31	-13.8	200.6	5.05	0.53
								NM	12.19	11.9	207.9	5.09	
26	Z ₂	Ni ₂ Pt ₂	0	1/3	1/3	-1/3	-1/3	FM	13.50	-34.2	209.3	5.10	0.45
								NM	13.40	-16.6	218.2	5.30	
27	Z ₃	NiPt ₃	1/4	1/3	2/3	0	1/3	FM	14.70	-53.5	223.8	5.20	0.42
								NM	14.62	-43.4	231.9	5.41	
28	L1 ₂	Ni ₃ Pt	1/4	0	1	0	1	FM	12.29	-69.4	201.8	4.92	0.59
								NM	12.17	-39.4	210.6	5.11	
								FM	12.12 ^f				
29	L1 ₂	NiPt ₃	1/4	0	1	0	1	FM	14.73	-64.3	228.9	5.48	0.27
								NM	14.69	-53.7	233.1	5.44	
								FM	14.53 ^f				
30	mC10	Ni ₄ Pt	9/25	1/3	1/5	1/3	1/3	FM	12.07	-27.8	200.1	5.10	0.57
31	mC10	NiPt ₄	9/25	1/3	1/5	1/3	1/3	FM	14.99	-27.6	226.1	5.38	0.33
32	D1 _a	Ni ₄ Pt	9/16	1/2	1/2	1/2	1	FM	12.01	-54.3	202.3	5.10	0.57
33	D1 _a	NiPt ₄	9/16	1/2	1/2	1/2	1	FM	14.99	-33.2	226.1	5.43	0.32
34	D1	Ni ₇ Pt	9/25	0	-1	0	1	FM	11.67	-24.8	198.9	5.00	0.59
35	D7	NiPt ₇	9/25	0	-1	0	1	FM	15.34	-29.5	234.9	5.51	0.23
36	ACS	Ni ₇ Pt	9/16	1/2	5/6	1/2	2/3	FM	11.61	-25.8	199.5	5.05	0.59
37	ACS	NiPt ₇	9/16	1/2	5/6	1/2	2/3	FM	15.30	-32.2	234.3	5.45	0.21
38	SQS-8	Ni ₆ Pt ₂	1/4	1/4	1/3	1/4	0	FM	12.32	-28.5	202.9	5.10	0.56
39	SQS-8	Ni ₄ Pt ₄	0	0	0	1/24	-1/12	FM	13.56	-57.5	210.7	5.27	0.49
40	SQS-8	Ni ₂ Pt ₆	1/4	1/4	1/3	1/4	0	FM	14.76	-39.0	223.1	5.22	0.41
41	SQS-16	Ni ₁₂ Pt ₄	1/4	1/4	1/4	1/4	5/24	FM	12.33	-29.8	202.5	5.11	0.56
42	SQS-16	Ni ₈ Pt ₈	0	0	0	0	0	FM	13.65	-39.2	211.8	5.28	0.50
43	SQS-16	Ni ₄ Pt ₁₂	1/4	1/4	1/4	1/4	5/24	FM	14.78	-35.2	224.9	5.41	0.36
44	SQS-32	Ni ₂₄ Pt ₈	1/4	1/4	1/4	1/4	1/4	FM	12.33	-32.7	201.6	5.10	0.57
45	SQS-32	Ni ₁₆ Pt ₁₆	0	0	0	0	0	FM	13.63	-42.6	211.8	5.27	0.50
46	SQS-32	Ni ₈ Pt ₂₄	1/4	1/4	1/4	1/4	1/4	FM	14.79	-30.0	224.6	5.53	0.35

^a See Appendix for the structure details, the $m+n$ in Ni_mPt_n indicates the independent atoms in the primitive cell.

^b Experimental data, see Table 2 for details.

^c Experimental data.⁵⁴

^d Experimental data.⁷

^e Experimental data at 298 K.⁵⁵

^f Experimental data.¹⁷

Figure captions

Fig. 1 (Color online) Average radial distribution functions (RDF's) for the SQS structures and the ideal fcc structure of FM Ni_{0.5}Pt_{0.5}.

Fig. 2 (Color online) Bond length distributions in the first nearest neighbor region of the disordered FM Ni_{1-x}Pt_x alloys predicted by first-principles SQS calculations. The dotted line indicates that the average bond length (mean value of SQS-8, SQS-16, and SQS-32) is equal to the bond length distribution. The solid lines indicate the average Ni-Ni, Ni-Pt, and Pt-Pt bond lengths according to SQS-32.

Fig. 3 (Color online) First-principles calculated equilibrium volumes (upper triangle) and bulk moduli (lower triangle) of the ordered and disordered (SQS's) FM Ni_{1-x}Pt_x alloys, see Table 4 for details.

Fig. 4 (Color online) First-principles calculated derivatives of bulk modulus relative to pressure (above panel) and magnetic moments (low panel) of the ordered and disordered (SQS's) FM Ni_{1-x}Pt_x alloys, see Table 4 for details. The experimental data are taken from Ref. 54.

Fig. 5 (Color online) First-principles calculated relative energies (i.e., formation enthalpies) of the ordered and disordered (SQS's) FM Ni_{1-x}Pt_x alloys when considering the FM contributions, see Table 4 for details. Note that the reference states are fcc Ni and fcc Pt, the dotted line links the ground states, the solid line is the CEM predicted results for disordered alloys based on the results of the ordered structures, the dashed line shows the fitted results by R-K polynomial for disordered alloys based on the SQS results, and the experimental data are from Ref. 55.

Fig. 6 (Color online) First-principles calculated phonon DOS's for the ordered and disordered (SQS's) FM Ni_{0.5}Pt_{0.5} alloys. The experimental data are derived from incoherent inelastic scattering.⁶²

Fig. 7 (Color online) First-principles calculated stretching and bending force constants of the ordered and disordered (SQS's) FM $\text{Ni}_{0.5}\text{Pt}_{0.5}$, together with the results for fcc Ni and fcc Pt (see Table 4 for the ordered structures used herein).

Fig. 8 (Color online) Predicted relative Helmholtz free energy (ΔF) and relative entropy (ΔS) of FM $\text{Ni}_{0.5}\text{Pt}_{0.5}$ between the ordered $L1_0$ and the disordered SQS-16 structures, with $L1_0$ being the reference state.

Fig. 1.

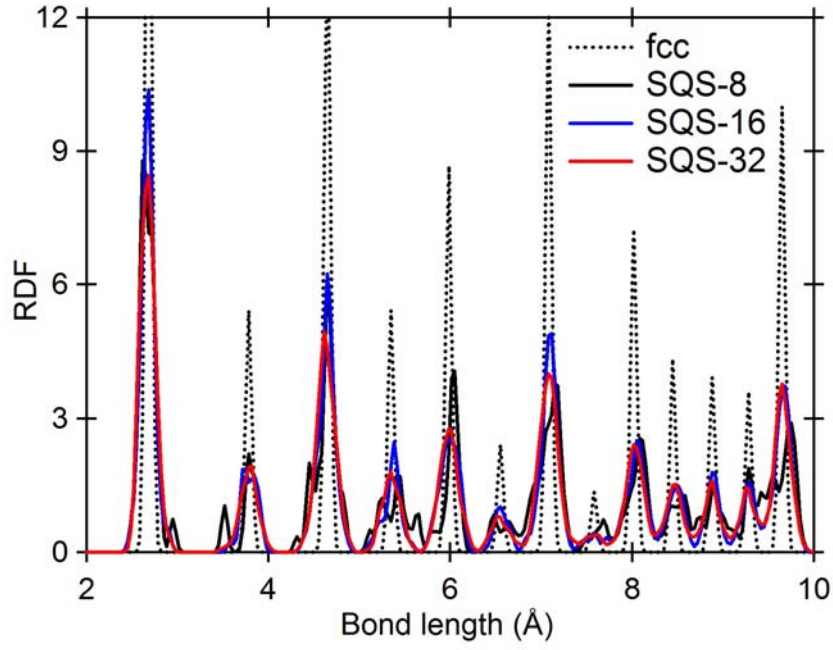


Fig. 2.

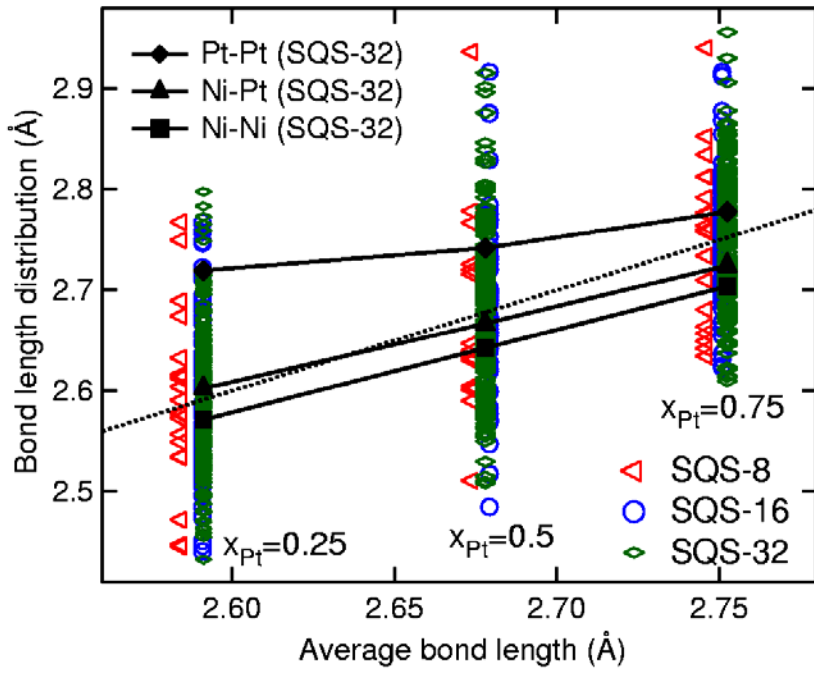


Fig. 3.

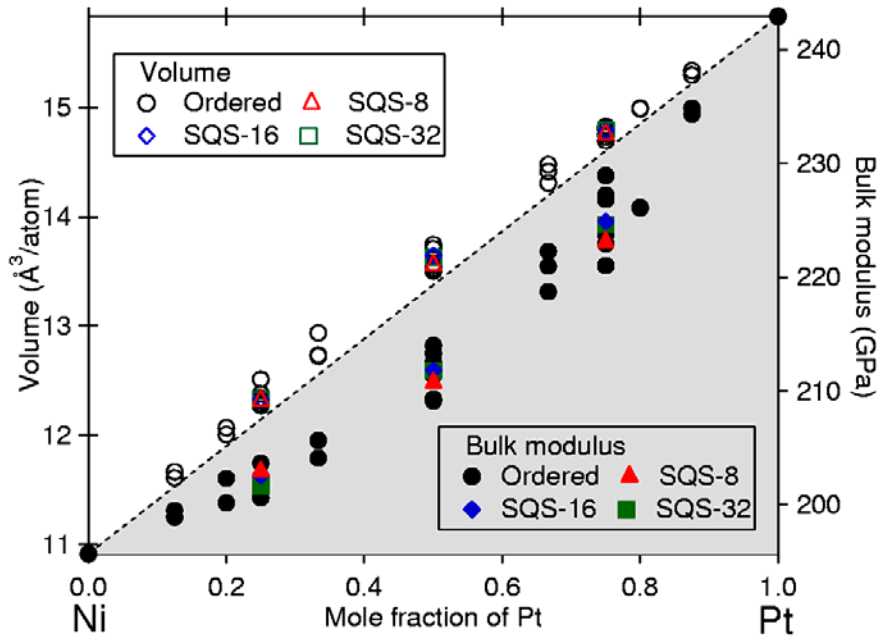


Fig. 4.

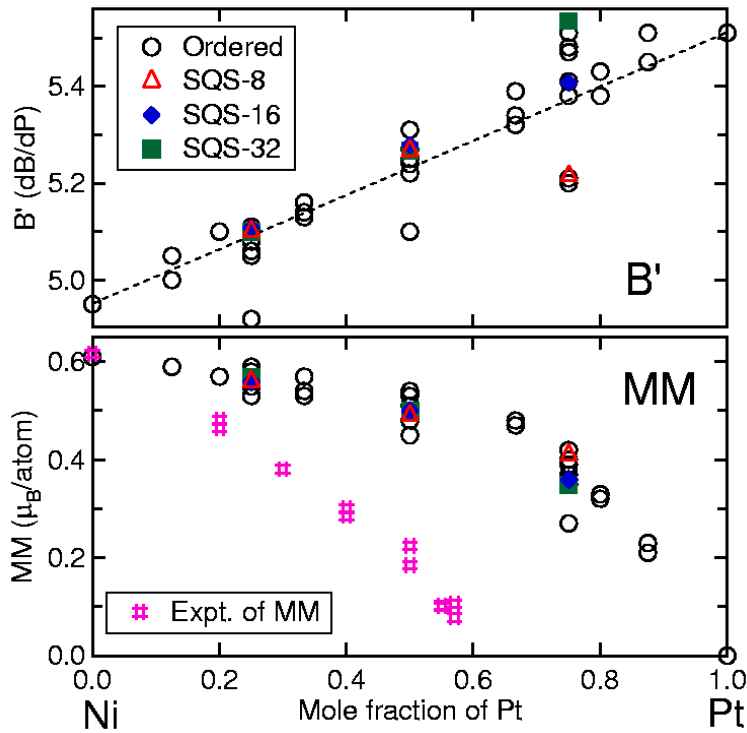


Fig. 5.

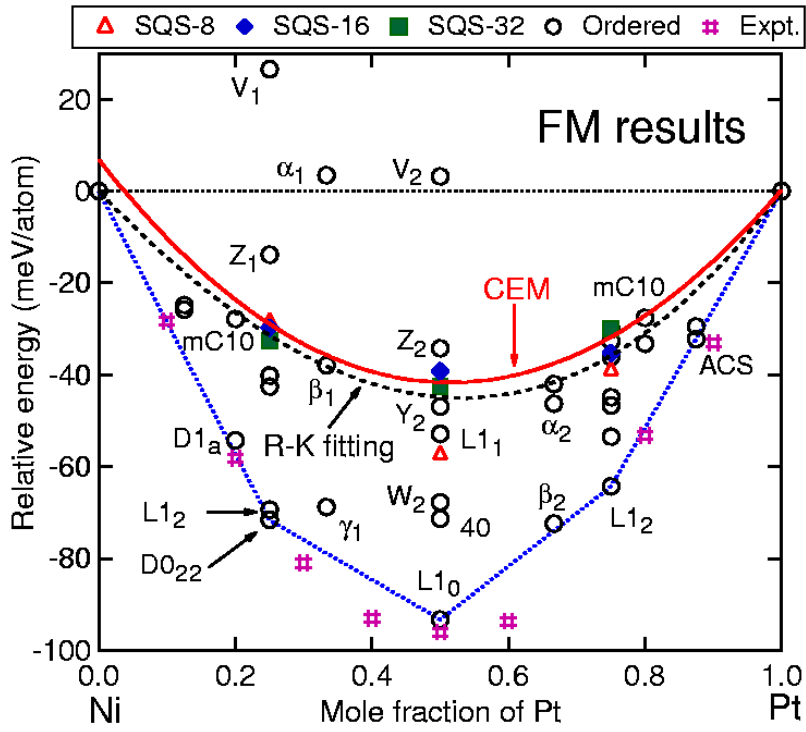


Fig. 6.

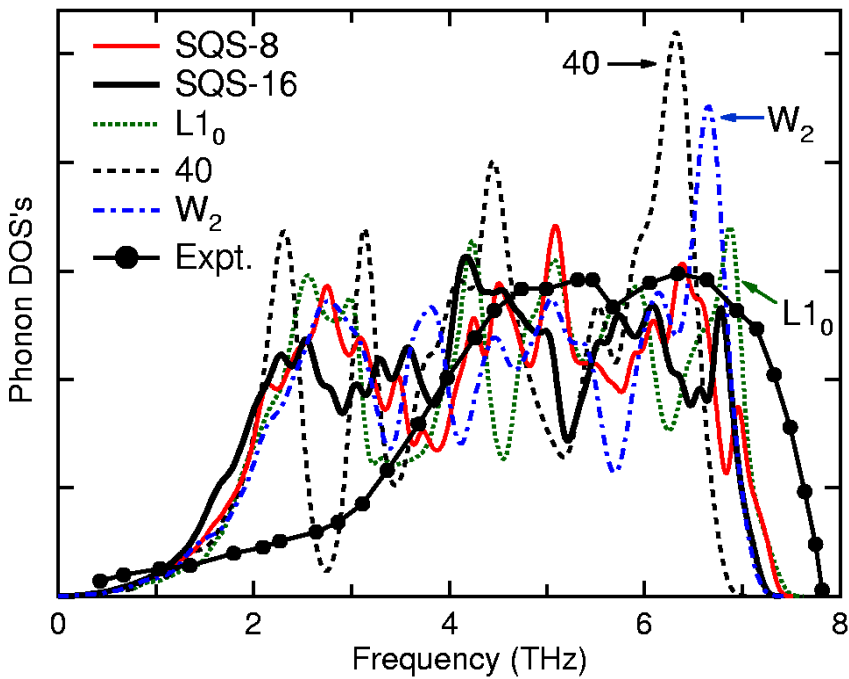


Fig. 7.

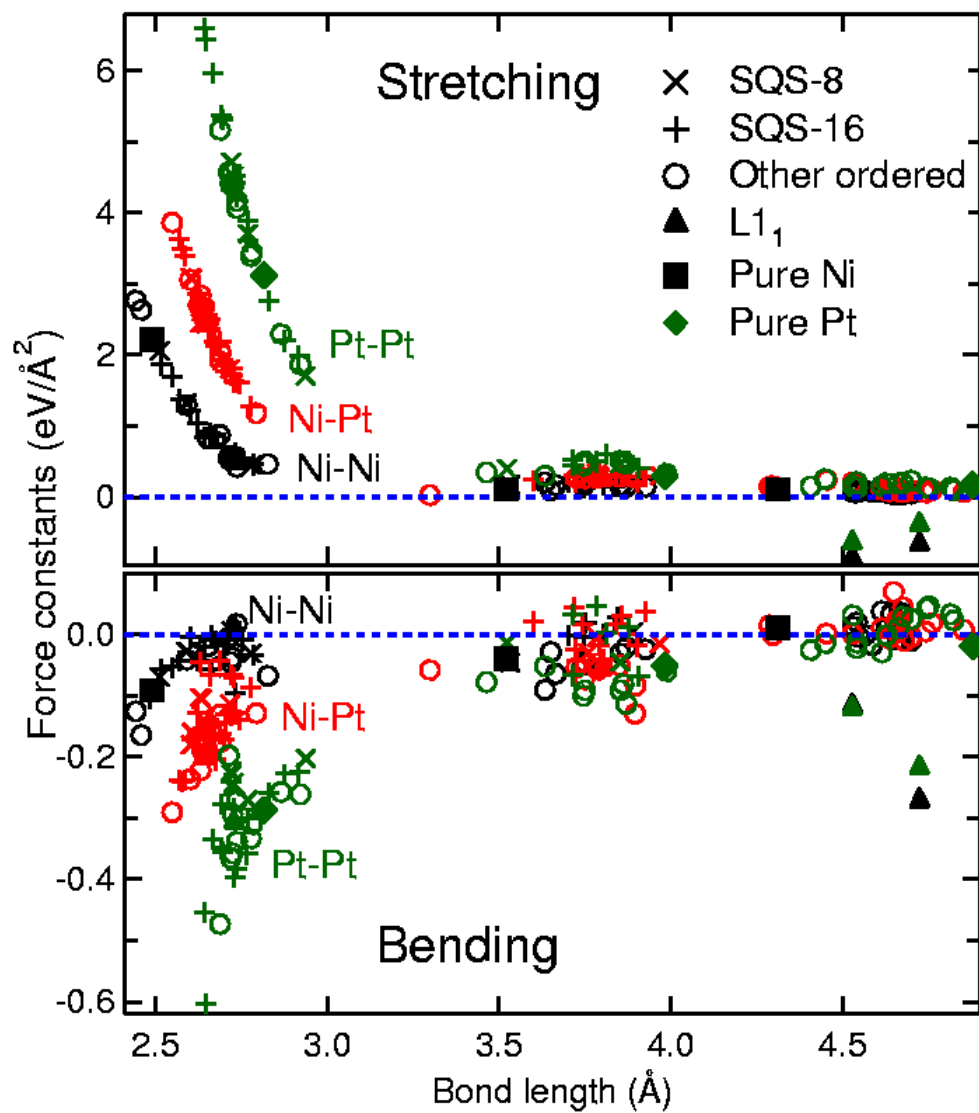
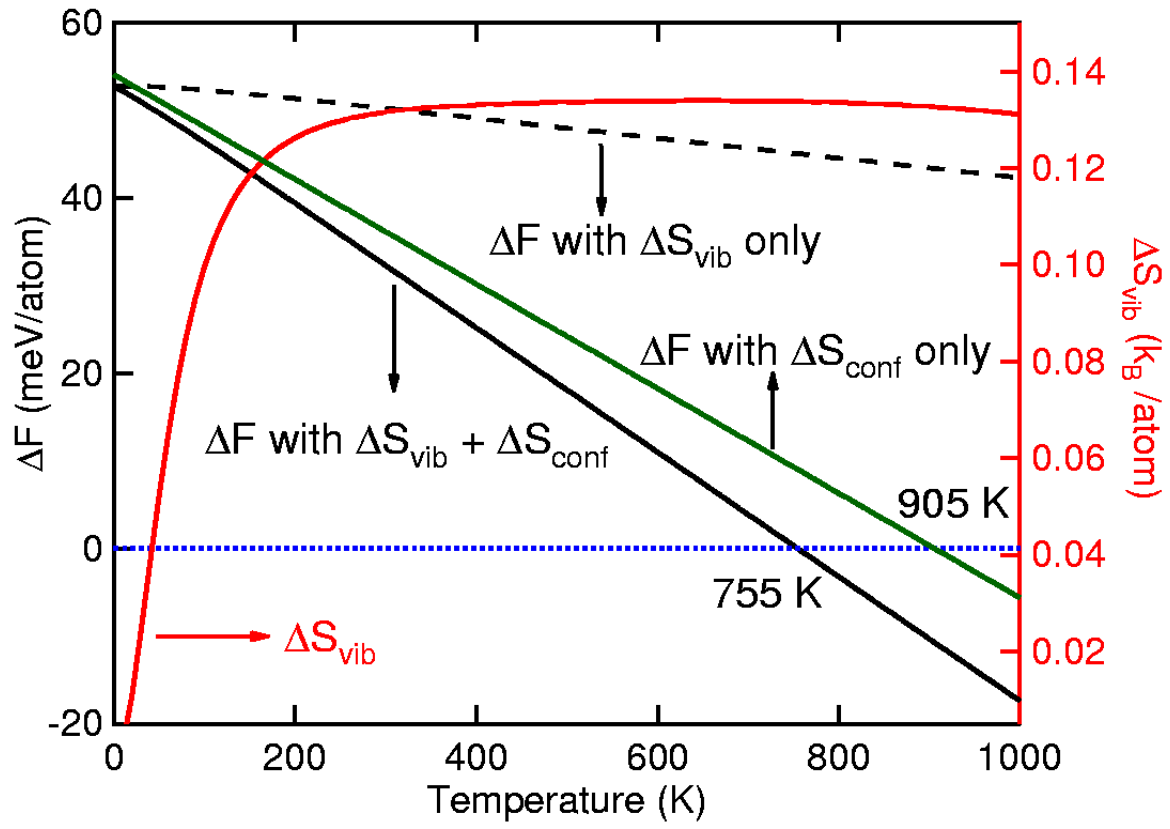


Fig. 8.



References and notes:

* Electronic address: sus26@psu.edu

- 1 D. R. Clarke and C. G. Levi, *Annu. Rev. Mater. Res.* **33**, 383 (2003).
- 2 N. P. Padture, M. Gell, and E. H. Jordan, *Science* **296**, 280 (2002).
- 3 D. S. Balint, T. Xu, J. W. Hutchinson, and A. G. Evans, *Acta Mater.* **54**, 1815 (2006).
- 4 A. W. Davis and A. G. Evans, *Metall. Mater. Trans. A* **37A**, 2085 (2006).
- 5 V. Deodeshmukh, N. Mu, B. Li, and B. Gleeson, *Surf. Coat. Tech.* **201**, 3836 (2006).
- 6 B. Gleeson, *J. Propul. Power* **22**, 375 (2006).
- 7 P. Nash and M. F. Singleton, *Bull. Alloy Phase Diagrams* **10**, 258 (1989).
- 8 G. Ghosh, A. van de Walle, and M. Asta, *Acta Mater.* **56**, 3202 (2008).
- 9 D. W. Taylor, *Phys. Rev.* **156**, 1017 (1967).
- 10 A. Zunger, S. H. Wei, L. G. Ferreira, and J. E. Bernard, *Phys. Rev. Lett.* **65**, 353 (1990).
- 11 P. Weightman, H. Wright, S. D. Waddington, D. Vandermarel, G. A. Sawatzky, G. P. Diakun, and D. Norman, *Phys. Rev. B* **36**, 9098 (1987).
- 12 G. Renaud, N. Motta, F. Lancon, and M. Belakhovsky, *Phys. Rev. B* **38**, 5944 (1988).
- 13 J. W. D. Connolly and A. R. Williams, *Phys. Rev. B* **27**, 5169 (1983).
- 14 S. L. Shang, Y. Wang, and Z. K. Liu, *Phys. Rev. B* **82**, 014425 (2010).
- 15 A. van de Walle and G. Ceder, *J. Phase Equilib.* **23**, 348 (2002).
- 16 S. Ghosh, P. L. Leath, and M. H. Cohen, *Phys. Rev. B* **66**, 214206 (2002).
- 17 S. Ghosh, J. B. Neaton, A. H. Antons, M. H. Cohen, and P. L. Leath, *Phys. Rev. B* **70**, 024206 (2004).
- 18 C. Jiang, C. Wolverton, J. Sofo, L. Q. Chen, and Z. K. Liu, *Phys. Rev. B* **69** (2004).
- 19 D. Shin, R. Arroyave, Z. K. Liu, and A. Van de Walle, *Phys. Rev. B* **74**, 024204 (2006).
- 20 Z. W. Lu, S. H. Wei, and A. Zunger, *Phys. Rev. B* **45**, 10314 (1992).
- 21 Z. W. Lu, S. H. Wei, and A. Zunger, *Phys. Rev. B* **44**, 10470 (1991).
- 22 A. van de Walle and G. Ceder, *Phys. Rev. B* **61**, 5972 (2000).
- 23 A. van de Walle, G. Ceder, and U. V. Waghmare, *Phys. Rev. Lett.* **80**, 4911 (1998).
- 24 C. K. Gan, Y. P. Feng, and D. J. Srolovitz, *Phys. Rev. B* **73**, 235214 (2006).
- 25 V. Ozolins and A. Zunger, *Phys. Rev. B* **57**, R9404 (1998).
- 26 C. Wolverton, *Acta Mater.* **49**, 3129 (2001).
- 27 A. V. Ruban, S. I. Simak, S. Shallcross, and H. L. Skriver, *Phys. Rev. B* **67**, 214302 (2003).
- 28 A. van de Walle, *CALPHAD* **33**, 266 (2009).
- 29 M. Sanati, L. G. Wang, and A. Zunger, *Phys. Rev. Lett.* **90**, 045502 (2003).
- 30 S. Curtarolo, D. Morgan, and G. Ceder, *CALPHAD* **29**, 163 (2005).
- 31 Z. W. Lu, S. H. Wei, A. Zunger, S. Frotapessoa, and L. G. Ferreira, *Phys. Rev. B* **44**, 512 (1991).
- 32 G. Kresse and J. Furthmuller, *Comput. Mater. Sci.* **6**, 15 (1996).
- 33 G. Kresse and J. Furthmuller, *Phys. Rev. B* **54**, 11169 (1996).
- 34 G. Kresse and D. Joubert, *Phys. Rev. B* **59**, 1758 (1999).
- 35 S. Shang, A. J. Bottger, M. P. Steenvoorden, and M. W. J. Craje, *Acta Mater.* **54**, 2407 (2006).
- 36 J. P. Perdew and Y. Wang, *Phys. Rev. B* **45**, 13244 (1992).
- 37 D. M. Ceperley and B. J. Alder, *Phys. Rev. Lett.* **45**, 566 (1980).

38 J. P. Perdew and A. Zunger, Phys. Rev. B **23**, 5048 (1981).
39 H. J. Monkhorst and J. D. Pack, Phys. Rev. B **13**, 5188 (1976).
40 M. Methfessel and A. T. Paxton, Phys. Rev. B **40**, 3616 (1989).
41 P. E. Blöchl, O. Jepsen, and O. K. Andersen, Phys. Rev. B **49**, 16223 (1994).
42 A. van de Walle and G. Ceder, Rev. Mod. Phys. **74**, 11 (2002).
43 A. van de Walle, M. Asta, and G. Ceder, CALPHAD **26**, 539 (2002).
44 S. L. Shang, Y. Wang, R. Arroyave, and Z. K. Liu, Phys. Rev. B **75**, 092101 (2007).
45 S. L. Shang, Y. Wang, and Z. K. Liu, Phys. Rev. B **75**, 024302 (2007).
46 S. L. Shang, Y. Wang, D. E. Kim, and Z. K. Liu, Comput. Mater. Sci. **47**, 1040 (2010).
47 Y. Wang, Z. K. Liu, and L. Q. Chen, Acta Mater. **52**, 2665 (2004).
48 P. Villars and L. D. Calvert, *Pearson's handbook of crystallographic data for intermetallic phases* (ASTM International, Newbury, OH, 1991).
49 S. L. Shang, Z. G. Mei, A. Saengdeejing, D. E. Kim, H. Zhang, S. Ganeshan, Y. Wang, and Z. K. Liu, Comput. Mater. Sci. **48**, 813 (2010).
50 G. Simmons and H. Wang, *Single Crystal Elastic Constants and Calculated Aggregate Properties* (MIT press, Cambridge (Mass.), 1971).
51 G. Kresse and J. Hafner, Phys. Rev. B **47**, 558 (1993).
52 S. L. Shang, Y. Wang, and Z. K. Liu, Appl. Phys. Lett. **90**, 101909 (2007).
53 S. L. Shang, G. Sheng, Y. Wang, L. Q. Chen, and Z. K. Liu, Phys. Rev. B **80**, 052102 (2009).
54 R. E. Parra and J. W. Cable, Phys. Rev. B **21**, 5494 (1980).
55 R. A. Walker and J. B. Darby, Acta Metall. **18**, 1261 (1970).
56 D. Paudyal, T. Saha-Dasgupta, and A. Mookerjee, J. Phys.: Condens. Matter **16**, 2317 (2004).
57 O. Redlich and A. T. Kister, Industrial and Engineering Chemistry **40**, 345 (1948).
58 Z. K. Liu, J. Phase Equilib. Diff. **30**, 517 (2009).
59 S. L. Shang, Y. Wang, Y. Du, and Z. K. Liu, Intermetallics **18**, 961 (2010).
60 B. Schonfeld, M. Engelke, and A. V. Ruban, Phys. Rev. B **79**, 064201 (2009).
61 X. L. Che, J. H. Li, Y. Dai, and B. X. Liu, Sci. China Ser. E **52**, 2681 (2009).
62 Y. Tsunoda, N. Kunitomi, N. Wakabayashi, R. M. Nicklow, and H. G. Smith, Phys. Rev. B **19**, 2876 (1979).
63 Y. Wang, S. L. Shang, X. D. Hui, L. Q. Chen, and Z. K. Liu, Appl. Phys. Lett. **97**, 022504 (2010).
64 S. L. Shang, L. G. Hector, Y. Wang, H. Zhang, and Z. K. Liu, J. Phys.: Condens. Matter **21**, 246001 (2009).
65 S. L. Shang, Y. Wang, H. Zhang, and Z. K. Liu, Phys. Rev. B **76**, 052301 (2007).
66 W. L. Bragg and E. J. Williams, Proc. R. Soc. London A **151**, 0540 (1935).
67 V. Ozolins, C. Wolverton, and A. Zunger, Phys. Rev. B **58**, R5897 (1998).
68 S. L. Shang, J. E. Saal, Z. G. Mei, Y. Wang, and Z. K. Liu, J. Appl. Phys. **180**, 123514 (2010).
69 Y. Wang, S. L. Shang, L. Q. Chen, and Z. K. Liu, Int J. Quantum Chem., doi:10.1002/qua.22865 (2011).
70 Y. Wang, S. L. Shang, H. Zhang, L. Q. Chen, and Z. K. Liu, Philos. Mag. Lett. **90**, 851 (2010).